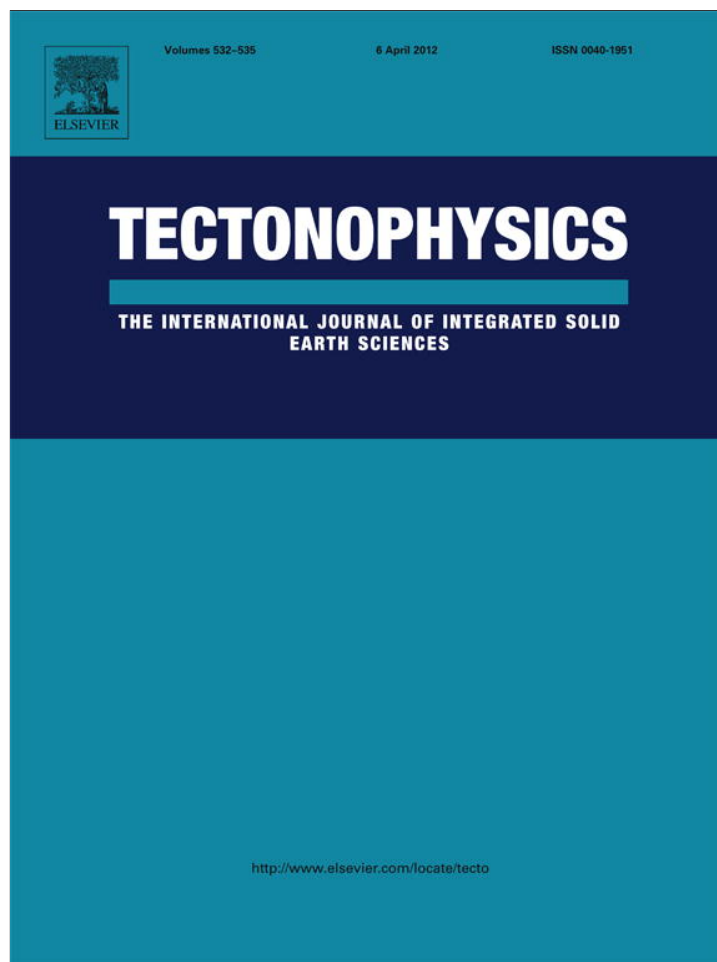


Provided for non-commercial research and education use.
Not for reproduction, distribution or commercial use.



This article appeared in a journal published by Elsevier. The attached copy is furnished to the author for internal non-commercial research and education use, including for instruction at the authors institution and sharing with colleagues.

Other uses, including reproduction and distribution, or selling or licensing copies, or posting to personal, institutional or third party websites are prohibited.

In most cases authors are permitted to post their version of the article (e.g. in Word or Tex form) to their personal website or institutional repository. Authors requiring further information regarding Elsevier's archiving and manuscript policies are encouraged to visit:

<http://www.elsevier.com/copyright>



Contents lists available at SciVerse ScienceDirect

Tectonophysics

journal homepage: www.elsevier.com/locate/tecto

Postseismic deformation mechanisms of the 1990 Mw 6.4 Gonghe, China earthquake constrained using leveling measurements

Ming Hao^{a,b}, Zheng-Kang Shen^{c,d,*}, Qingliang Wang^b, Duxin Cui^b

^a State Key laboratory of Earthquake Dynamics, Institute of Geology, China Earthquake Administration, Beijing 100029, China

^b Second Monitoring Center, China Earthquake Administration, Xi'an 710054, China

^c School of Earth and Space Science, Peking University, Beijing 100871, China

^d Dept. of Earth and Space Sciences, University of California, Los Angeles, CA 90095-1567, USA

ARTICLE INFO

Article history:

Received 2 June 2011

Received in revised form 25 December 2011

Accepted 5 February 2012

Available online 18 February 2012

Keywords:

Gonghe earthquake

Leveling measurements

Postseismic deformation

Afterslip

Viscoelastic relaxation

ABSTRACT

We model leveling deformation data observed following the 1990 Mw 6.4 Gonghe earthquake in Qinghai province, western China, to infer postseismic deformation sources and mechanisms. Using coseismic vertical displacements and previous study result obtained from seismic body wave inversion, we update the main shock rupture model as a reverse dip-slip of 0.81 m. Analyzing the leveling data observed one time before and six times after the quake across the seismic fault, we find that: (1) the near-field deformation at the hanging-wall side of the coseismic rupture continued to uplift over a large region after the earthquake, with the highest rate measured in the first year; (2) the scope of the postseismic doming region coincides with the coseismic doming region; (3) time series of elevation change between adjacent benchmarks can be modeled by a logarithmic or an exponential relaxation function, with the relaxation time constants estimated as 0.165 years and 1.344 years for the two models, respectively. To model the postseismic displacements, we utilize the raw observations of elevation differences between adjacent benchmarks, not their integrals with respect to a reference benchmark, to constrain a dislocation model in a continuum. It makes full use of the leveling data and effectively reduces biases introduced from cumulative errors due to data integration. Our postseismic modeling result suggests that two mechanisms operate simultaneously to produce the postseismic vertical deformation observed at the surface: afterslip on the coseismic rupture fault plane of the main shock and its peripheral extension, particularly upward into the sediment layer above the main rupture, and viscoelastic relaxation of the lower crust and upper mantle, with a viscosity of 9×10^{19} Pa·s. The result suggests more brittle and less viscous lower crust and upper mantle underneath the Qaidam basin than some of previous studies envisioned.

© 2012 Elsevier B.V. All rights reserved.

1. Introduction

The Mw 6.4 Gonghe earthquake of 26 April 1990 occurred in Qinghai Province, western China. Epicenter of the earthquake was located in the southern edge of the Gonghe basin, northeast Tibetan Plateau (Fig. 1). The quake did not break to the surface, and formation of the seismogenic structure has been controversial due to complexity of regional tectonics. Most people believed that the Gonghe earthquake ruptured a buried fault trending WNW (e.g. Tu, 1992). According to Tu (1992), the seismogenic fault (black line in Fig. 2) starts from the west of Chaka Salt Lake, goes through Waxiangyuka and Tanggemu, and ends at the Mangla valley where the Yellow river runs through. Chen et al. (1996) and Li and Chen (1996) inverted leveling and seismic body wave data to determine the seismic source and rupture process of the quake. Their results revealed that P-axis of the quake was close to

horizontal and oriented NNE, which was indicative of the regional direction of the maximum compressional stress, and consistent with the relative convergence direction between the Indian and Eurasian plates.

After the Gonghe earthquake the China Earthquake Administration dispatched a survey team which made repeated leveling surveys along two leveling routes passing through the epicentral region. These data, as presented in the latter part of this paper, show significant postseismic deformation signals. Such data provide us opportunities to investigate the deformation sources and physical mechanisms, and the result helps us better understand the friction properties of the seismogenic fault and viscoelastic structure of the media, and may provide fundamental constraints for geodynamic modeling of the lithosphere.

Because coseismic strike-slip along the fault is somewhat controversial (Li and Chen, 1996; Wang and Wang, 1998; Xu and Chen, 1997; Zhao et al., 1992), in this study we also investigate the coseismic slip distribution, and the result is used as the initial driving force for our subsequent modeling of postseismic deformation. We then examine the temporal and spatial characteristics of the leveling postseismic deformation field. We describe the characteristics of

* Corresponding author at: School of Earth and Space Science, 2825 Second Science Building, Peking University, Beijing 100871, China. Tel./fax: +86 10 62754037.
E-mail address: zhengkangshen@pku.edu.cn (Z.-K. Shen).

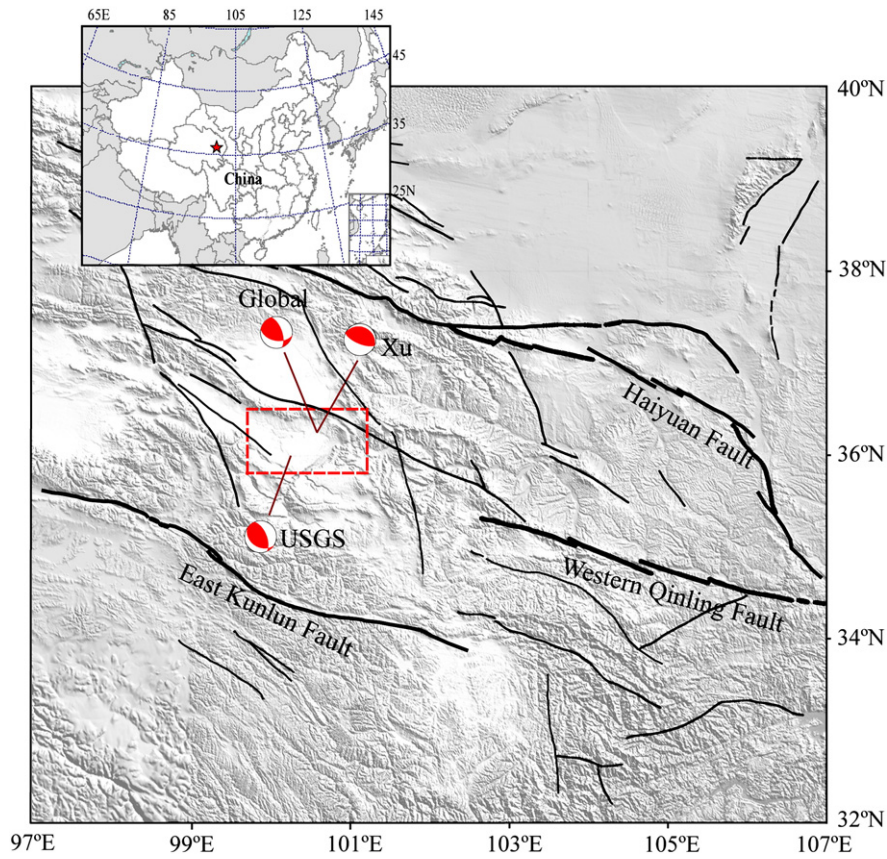


Fig. 1. Tectonic map of northeast Tibetan Plateau. Inset map shows the location of the studied region in China. Thick black lines are the main active faults and thin lines are the minor faults in the region. A rectangle outlined by red dashed lines denotes the Gonghe area shown in Fig. 2. Focal mechanism solutions are from the United States Geological Survey, Global CMT, and Xu and Chen (1997), respectively.

postseismic vertical deformation using logarithmic and exponential relaxation functions and estimate their time constraints. At last, we employ a model combining fault afterslip with lithospheric viscoelastic relaxation and constrained by the leveling data to study the source and mechanism of the postseismic deformation.

2. Leveling data

A first order leveling survey was initially conducted by the State Bureau of Surveying and Mapping along two leveling routes (Daohua and Shitang) in the Gonghe basin in 1978. The 1990 Gonghe

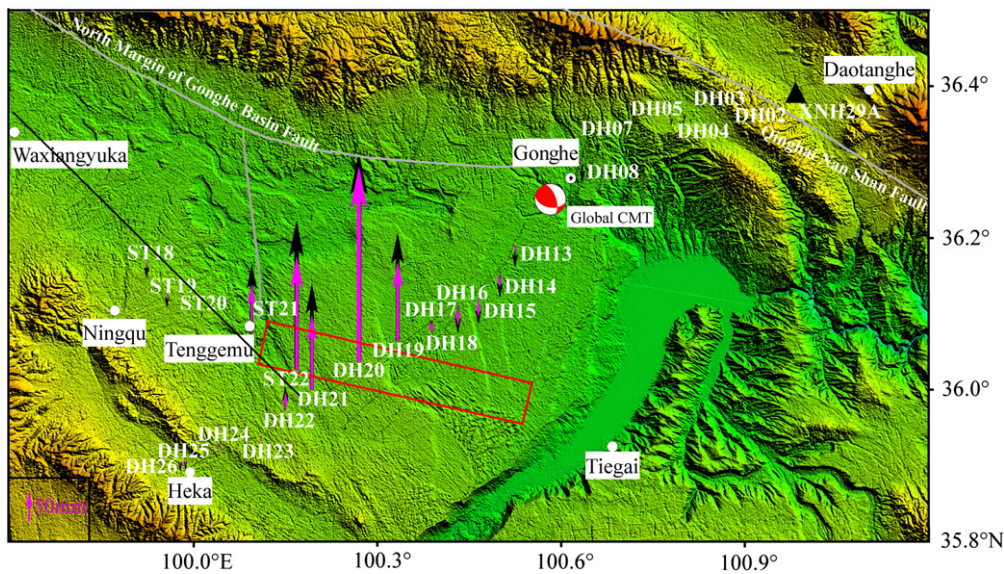


Fig. 2. Observed and model-predicted coseismic vertical displacements of the Gonghe earthquake (relative to the benchmark XNH29A shown as a black triangle). Black arrows stand for vertical displacements derived from pre- and post-seismic leveling measurements. Pink arrows are coseismic displacements predicted by model. The leveling routes were measured from XNH29A westward. The black line is the seismogenic fault suggested by Tu (1992). The red outlined rectangle is the surface projection of the fault rupture given by this study.

earthquake occurred in the neighborhood of the two leveling routes. After the quake, the Second Monitoring Center of China Earthquake Administration carried out first order leveling surveys along the two routes (Fig. 2) repeatedly in May 1990, May and October 1991, August 1992, June 1994, and July 1995, to closely monitor postseismic deformation of the Gonghe earthquake.

Leveling data observed in 1978 and May 1990 provide direct measurements of coseismic vertical displacements (Fig. 2). Vertical coseismic displacements along the Daohua route (whose benchmarks are named using “DH” as initials) as shown in Fig. 2 demonstrate doming between benchmarks DH18 and DH23 and peaked at DH20, which uplifted 345 mm relative to XNH29A. In addition, the doming is symmetric, and the deformation gradients at both flanks are ~28 mm/km. Northeast of the doming is a subsidence region centered around the benchmark DH16, which subsided up to 45.2 mm relative to XNH29A. As shown in Fig. 2, another dome is centered around the benchmark ST22 along the Shitang route (whose benchmarks are named using “ST” as initials), with the benchmark uplifted 246.6 mm relative to XNH29A, and the deformation gradients at the two flanks of the dome are about 14.6 mm/km. From the vertical displacements of these two leveling routes we can see that uplift at benchmark DH20 is the highest, displacements along the leveling routes decline more and with greater subsidence to the Gonghe and Heka direction than to the Tanggemu direction.

Fig. 3 shows the vertical displacements of the two leveling routes in the first year after the quake, which reveals that postseismic uplift is more broadly distributed than coseismic uplift, while the postseismic doming region coincides with the coseismic doming region. The postseismic doming region is between the benchmarks DH16 and DH22 along the Daohua route, and between DH16 and ST20 for the Shitang route, respectively. It centers at DH19 with the mean uplift rate reaching 63.5 mm/year relative to the benchmark XNH29A. Moreover, the highest uplift shifted from the benchmark DH20 for coseismic to the benchmark DH19 for postseismic deformation, with the latter benchmark located about 6 km east of the former benchmark.

The vertical displacements measured in the following years show a deformation pattern similar to that of the first year after the quake, but with smaller amplitudes (Fig. 4). Close examination of the spatio-temporal deformation pattern following the Gonghe earthquake reveals that: (1) The postseismic deformation is dominated by uplifting, which decays gradually with time; (2) the postseismic doming area is spatially invariant over the years, but is greater than the coseismic uplift region; and (3) comparing to the coseismic uplifting, center of the postseismic doming region moved ~9 km eastward, from near the benchmark of DH20 to DH19.

3. Inversion of coseismic slip distribution

Postseismic deformation is excited by coseismic deformation, thus postseismic deformation modeling requires fault geometry and a focal mechanism solution to provide the initial driving source. However, due to the lack of horizontal geodetic data constraints and the complexity of rupturing process, focal mechanism solutions of the Gonghe earthquake obtained in previous studies are not without controversy (Li and Chen, 1996; Wang and Wang, 1998; Xu and Chen, 1997; Zhao et al., 1992). Zhao et al. (1992) inverted leveling data to

Table 1
Fault rupture parameters of Gonghe earthquake.

Length (km)	Width (km)	Strike (°)	Dip (°)	Rake (°)	Slip (m)	Coordinate of upper left corner of fault plane		
						ϕ (°)	λ (°)	d (km)
40	10.7	102	48	89	0.81	36.09	100.12	4.05

Table 2
Logarithmic relaxation amplitudes of elevation difference time series.

Baseline	Adjusted D_i (mm)	Predicted D_i (mm)	Baseline	Adjusted D_i (mm)	Predicted D_i (mm)
DH08-DH13	0.60 ± 0.70	-0.18	DH21-DH22	-15.96 ± 2.19	-1.18
DH13-DH15	-1.57 ± 0.35	-0.44	DH22-DH23	0.91 ± 0.11	0.11
DH15-DH16	-1.30 ± 0.14	-0.37	DH23-DH24	0.27 ± 0.40	0.17
DH16-DH17	8.35 ± 0.29	-0.70	DH24-DH25	1.65 ± 0.32	0.13
DH17-DH18	0.85 ± 0.02	0.85	DH25-DH26	0.05 ± 0.002	0.01
DH18-DH19	15.92 ± 0.48	17.53	DH21-ST22	12.58 ± 2.38	2.84
DH19-DH20	-5.90 ± 0.23	-5.10	ST22-ST21	-15.51 ± 3.20	9.02
DH20-DH21	-6.67 ± 1.24	-10.97	ST21-ST20	-10.94 ± 0.55	-9.76

determine the fault rupture parameters of the Gonghe earthquake, and determined that the quake was caused by reverse faulting on a dip-slip fault with a small left-lateral component. Li and Chen (1996) and Xu and Chen (1997) used seismic body waves to constrain the earthquake rupture mechanism and obtained reverse faulting on a dip-slip fault with a large left-lateral component. Their result also suggested that the main shock was composed of at least two events. Wang and Wang (1998), however, used the same leveling data as that of Zhao et al. (1992) as model constraints, and concluded that the coseismic fault is a reverse dip-slip with a dextral component. Therefore, we try to employ a single rectangular fault to invert for the fault geometry and amount of slip, using Okada's elastic dislocation model for Green's function computation (Okada, 1992).

We assume uniform slip on fault, and use the coseismic leveling data as constraints solving for fault slip model parameters. The solution is obtained in two steps, in the first step 8 model parameters: upper left position of the fault plane (latitude, longitude, and depth), fault length, width, strike, dip, and up-dip component of slip are estimated through a grid search. The strike-slip component of slip is not solved for in this step because: (a) it is not well constrained by the leveling data, and (b) it is much smaller than the up-dip component based on seismic studies (e.g. <http://www.globalcmt.org/CMTsearch.html>; Li and Chen, 1996; Person, 1991; Xu and Chen, 1997), and omitting it in this step should not have much effect on estimation of other parameters. In group search we minimize the postfit residual χ^2 using the weighted least-squares method:

$$\chi^2 = \sum_{i=1}^N w_i (s_i^o - s_i^c)^2 \quad (1)$$

where N is the total number of data entry, w_i is the weight of the i -th observation (reciprocal of the square of data uncertainty), and s_i^o and s_i^c are the i -th observed and calculated crustal displacement, respectively.

We divide the 7 geometric parameters into two groups. The first group includes 3 parameters defining the upper left position of the fault plane, which is searched for while constraining the 4 second group parameters to the ones given by Zhao et al. (1992). Next the first group parameters are fixed to the optimal values and the second group parameters (fault strike, dip, length, and width) are searched. After obtaining optimal values of the second group parameters, a global search is conducted again for all the 8 parameters in the vicinity of the current solution, to warrant achieving the global minimum of the postfit residual χ^2 . The final result indicates that the fault is in the length of 40 km and width of 10.7 km, with the strike and dip angles as 102° and 48° respectively. In the second step the fault rupture is allowed to have a strike slip component, and its optimal value is searched for. We start with a slip rake angle of 89° following the result of Xu and Chen (1997) obtained from seismic waveform data inversion, and search for the amplitude of slip. We then retain the dip-slip component at 0.814 m and search for the strike-slip component.

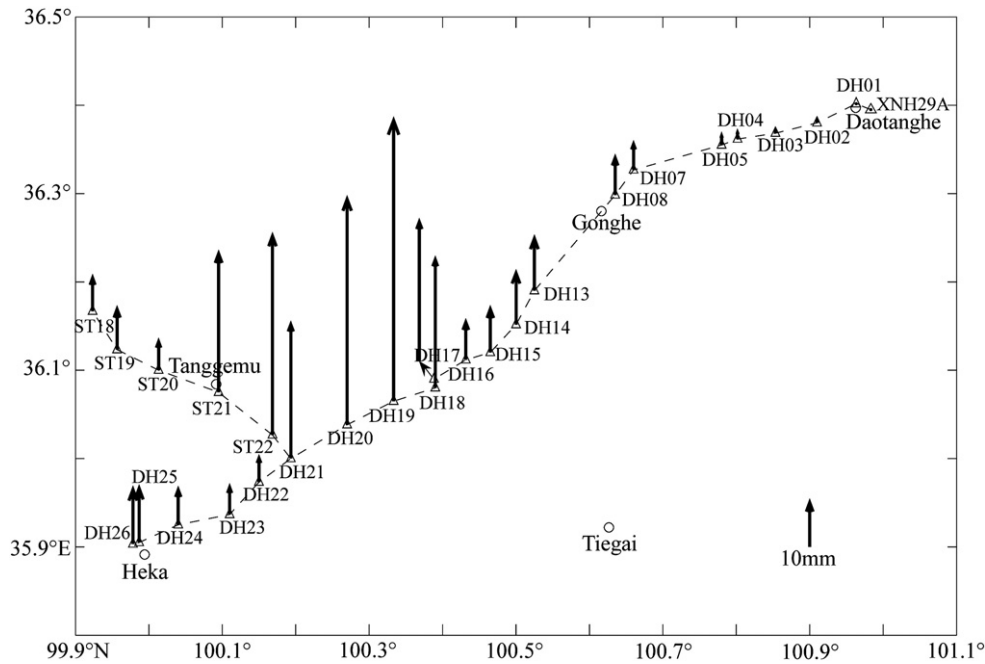


Fig. 3. First year (1990.4–1991.4) vertical displacements after the earthquake (relative to benchmark XNH29A).

The result yields 0.014 m left-slip, with the minimum of reduced postfit χ^2 as 558 m². Table 1 lists the inverted fault rupture parameters. Fig. 2 shows that the observed coseismic displacements (black arrows) fit our model (pink arrows) well.

4. Temporal behavior of postseismic deformation

Time series data of elevation change between adjacent benchmarks illustrate that most of the benchmarks had vertical movements since the earthquake (Fig. 4). Such vertical movements are considered rheological responses of the fault and crust to coseismic stress changes. In such a case two simple models are often adopted to describe the rheological behavior of fault zone rocks: logarithmic and exponential relaxation functions

$$h(t) = D_l \log(1 + t/\tau_l) \quad (2)$$

$$h(t) = D_e(1 - \exp(-t/\tau_e)) \quad (3)$$

where $h(t)$ is the elevation change between two adjacent benchmarks, τ_l and τ_e are the relaxation time constants for logarithmic and exponential models, and D_l and D_e are the amplitudes of relaxation (Shen et al., 1994). The term t is the time after the earthquake.

We estimate the relaxation constants τ_l and τ_e using data between adjacent benchmarks involving sites DH15, DH16, DH17, DH18, and DH20. These benchmarks have long occupation history and show clear postseismic deformation. We assume that τ_l and τ_e are the same for all the observations, i.e. the postseismic signals are to have the same temporal behavior and share a common deformation origin. Validity of this assumption is to be verified later in our study. Each adjacent station pair is assumed to have its own postseismic amplitude D_l or D_e , which are estimated using the least-squares adjustment of the data. Multiple adjustments are performed, each time assuming a relaxation time constant, and the best estimate of the relaxation

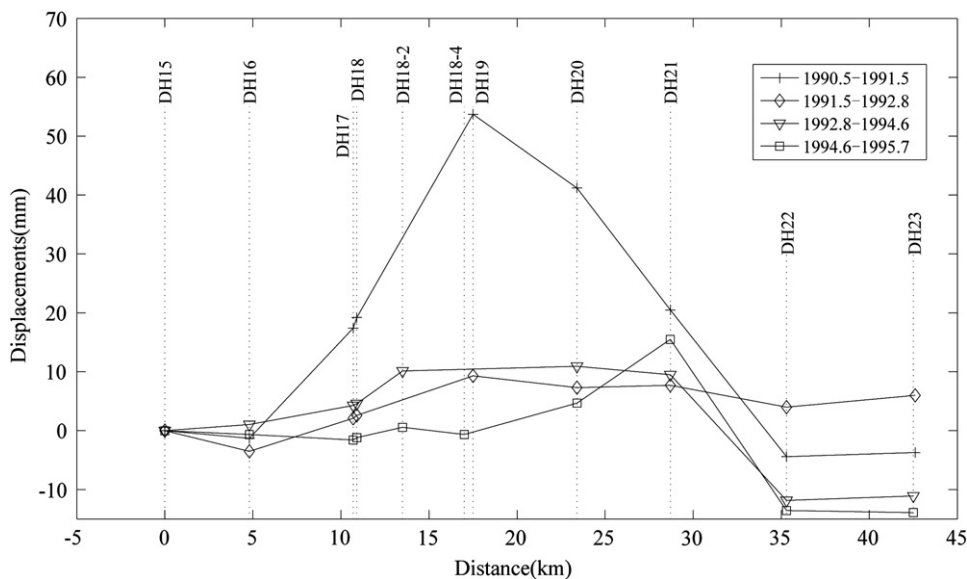


Fig. 4. Postseismic vertical displacements 1990–1995 after the Gonghe earthquake (relative to the benchmark DH15).

time constant is the one with the least χ^2 of the postfit residuals. Our result indicates that the logarithmic relaxation time τ_l is about 0.165 year ($0.082 \text{ year} < \tau_l < 0.289 \text{ year}$ at the 95% confidence level estimated using the F-test) and the exponential relaxation time τ_e about 1.344 years ($1.106 \text{ years} < \tau_e < 1.632 \text{ years}$ at the 95% confidence level). The data postfit residual χ^2 of the logarithmic and exponential models are 4387.3 and 4668.1 mm^2 respectively, indicating that the two models fit the observation data about equally well. We then adopt the best estimated relaxation time constant in relaxation model and deduce amplitudes of all the elevation changes between two adjacent benchmarks using least squares adjustment. The data fitting results of logarithmic and exponential relaxation models are shown in Fig. 5.

5. Physical mechanism of postseismic deformation

Generally speaking, there are two kinds of physical models to describe regional scale postseismic deformation. In one model, viscoelastic relaxation is assumed to occur throughout the lower crust and upper mantle (Nur and Mavko, 1974; Pollitz, 1997; Reilinger, 1986). In the other model, deformation is resulted from afterslip on the fault plane (Marone et al., 1991; Shen et al., 1994; Ueda et al., 2001). Different mechanisms of postseismic deformation tend to show different characteristics, reflecting the rheologic process of the fault zone. In this paper we attempt to explore the dominant source of postseismic deformation following the Gonghe earthquake, the

result may shed lights on crustal structure and seismo-tectonic process of the region.

5.1. Afterslip model

Previous studies showed that afterslip tend to occur on the same fault plane and within and beyond the scope of the coseismic rupture (e.g. Bürgmann et al., 2002; Owen et al., 2002; Shen et al., 1994). We employ a model with a single rectangular fault segment coinciding with the coseismic fault plane, and assume that fault slip rate is uniform on the fault plane, and the slip rate decays logarithmically with time. The strike, dip, and geometric origin of the fault plane are constrained using the parameters from the inversion of coseismic slip, and four parameters: the east, west, updip, and downdip edge distances measured from the origin are left to be estimated (see Fig. 6 for the setting of fault plane geometry). We invert the amplitudes of logarithmic functions of elevation difference between adjacent benchmarks for amplitude of afterslip on fault. We start with an initial fault rupture model obtained earlier in Section 2, and conduct a grid search to find the scope and amount of afterslip in the model that minimizes Eq. (1).

For the observed displacements s_i^0 , $i = 1, \dots, N$ in Eq. (1), the conventional approach is to get the elevation differences of all the benchmarks with respect to a reference benchmark. Having acquired relative elevations of all the benchmarks in the initial survey, the following postseismic surveys would deduce elevation changes of the

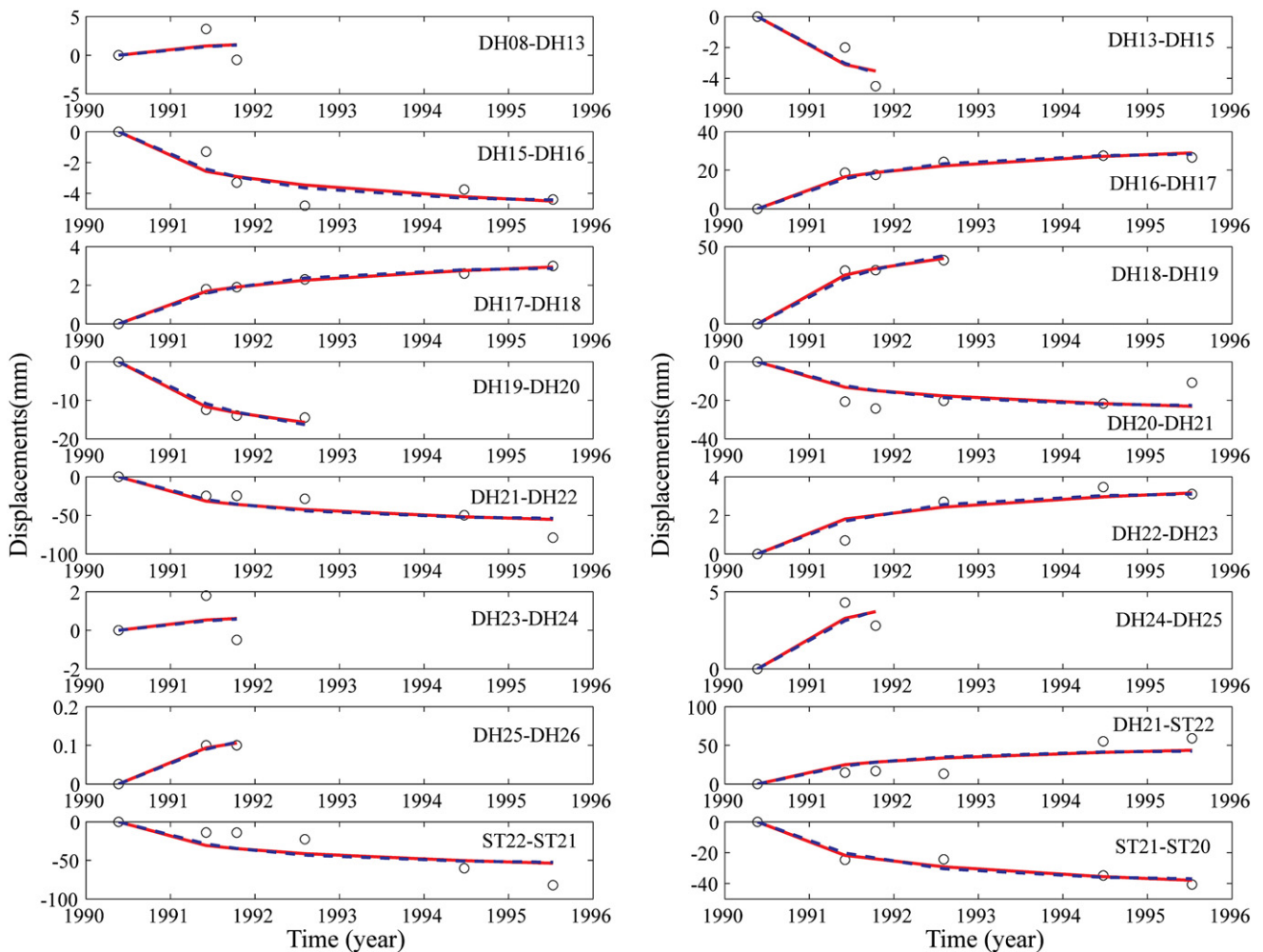


Fig. 5. Data fitting results of logarithmic and exponential relaxation model. τ_l and τ_e are 0.165 and 1.344 years respectively. Circles are the measured elevation changes, and red solid lines and blue dashed lines are data fitting results using logarithmic and exponential models respectively.

benchmarks relative to their initial elevations. There are three drawbacks in this approach. First, errors are accumulative along the survey routes; if the route is long, elevations measured at benchmarks distant from the reference can become quite large. Second, data quality relies heavily on the quality of the reference benchmark; if the reference benchmark is not stable or disturbed during the survey time period, the entire dataset will be biased. Third, data from repeated surveys can be fully used only if the surveys follow exactly the same route as the initial survey, otherwise measurements made along different survey routes will not have common benchmarks to derive the elevation changes.

We adopt an unconventional approach using leveling data to investigate the source and mechanism of postseismic deformation. This approach utilizes the raw observations of elevation differences between adjacent benchmarks, not their integrals with respect to a reference point, to constrain a dislocation model, effectively reducing biases introduced from cumulative errors due to data integration and making full use of the leveling data. We invert amplitudes D_i (or D_e) described in Section 4 to define afterslip on fault, adopting Okada's elastic dislocation model for Green's function computation (Okada, 1992). The leveling survey is relatively less sensitive to horizontal deformation produced by strike-slip motion on fault. Nevertheless, since this earthquake was primarily a reverse faulting event, it is reasonable to assume that afterslip motion was also dominated by thrust motion, and the strike-slip motion on fault was zero. A grid search is performed to obtain optimal values of the five parameters, of which four are edge distances and one is the up-dip component of slip, determined from data postfit residual χ^2 evaluation. Relative to the four fault rupture boundaries of the coseismic slip model, our result shows that the afterslip fault plane moved northwestward, with the west boundary moved 7.3 km (1.3–10.1 km at the 70% confidence level) and the east boundary 14.8 km (8.1–17 km at the 70% confidence level) westward along the fault, respectively. The upper and lower boundaries moved 2.8 km (2.4–3.2 km at the 70% confidence level) and 5.5 km (3.8–7 km at the 70% confidence level) upward along the fault, respectively (Fig. 6). The afterslip fault plane therefore is 32.5 km long along strike and 8 km wide, with the top edge 2.0 km underneath the surface. The amplitude of dip-slip on the fault is 0.043 ± 0.006 m. The postfit residual χ^2 for the afterslip model is 1608.1 mm^2 , and the reduced postfit residual χ^2 is 146.2 mm^2 . The estimated relaxation amplitudes of two adjacent benchmarks and the afterslip model are shown in Table 2 and Fig. 7.

We can forward predict the time series of elevation differences between adjacent benchmarks using inverted relaxation amplitudes and time function of Eq. (2). Fig. 8 shows the comparison between elevation differences (circles) and afterslip model results (crosses), the χ^2 of postfit residuals is 23876.1 mm^2 , and the reduced postfit residual χ^2 is 341.1 mm^2 .

5.2. Viscoelastic relaxation model

It is evident from Figs. 7 and 8 that although the afterslip model can interpret most part of the leveling data, there is still a significant amount of postfit residuals left not explained, particularly for baselines DH16–DH17, DH21–22, DH21–ST22, and ST22–ST21. We therefore try to model the dataset differently, adopting a viscoelastic relaxation model realized using the code of PSGRN/PSCMP (Wang et al., 2006). A flat layered earth is assumed, and a standard linear solid model (i.e. clustering of a Kelvin material and an elastic string) is used to describe the viscoelasticity of the media (Shi et al., 2006). Table 3 shows a 2-layer crustal structure model of the Gonghe region (after Li and Chen, 1996), where the depth range of upper crust H and the viscosity η in the lower crust and upper mantle are elected as unknown parameters.

We conduct a grid search to find the best fit values of the unknown model parameters H and η . During each trial a set of parameters of H and η are assumed, and the coseismic slip model obtained in Section 3 is imposed as the initial condition to drive the system to deform mechanically. The elevation differences between benchmarks are predicted at various epochs, and compared with the data to derive data postfit residual χ^2 . The objective is to find a solution which minimizes Eq. (1). The search ranges are 10–30 km for H in steps of 0.5 km, and 10^{18} – $10^{21} \text{ Pa}\cdot\text{s}$ for η in steps of $10^{18} \text{ Pa}\cdot\text{s}$ for 10^{18} – $10^{19} \text{ Pa}\cdot\text{s}$, $10^{19} \text{ Pa}\cdot\text{s}$ for 10^{19} – $10^{20} \text{ Pa}\cdot\text{s}$, and $10^{20} \text{ Pa}\cdot\text{s}$ for 10^{20} – $10^{21} \text{ Pa}\cdot\text{s}$, respectively.

For two adjacent benchmarks i and j , the elevation differences between them at the time t_0 immediately after the earthquake and at a later time t are $h_{ij}(t_0)$ and $h_{ij}(t)$ respectively. Hence, the postseismic changes of elevation difference between benchmarks i and j at the time t is

$$h_{ij} = h_{ij}(t) - h_{ij}(t_0) \quad (4)$$

In reality we can hardly acquire $h_{ij}(t_0)$, but $h_{ij}(t)$ can be measured by leveling.

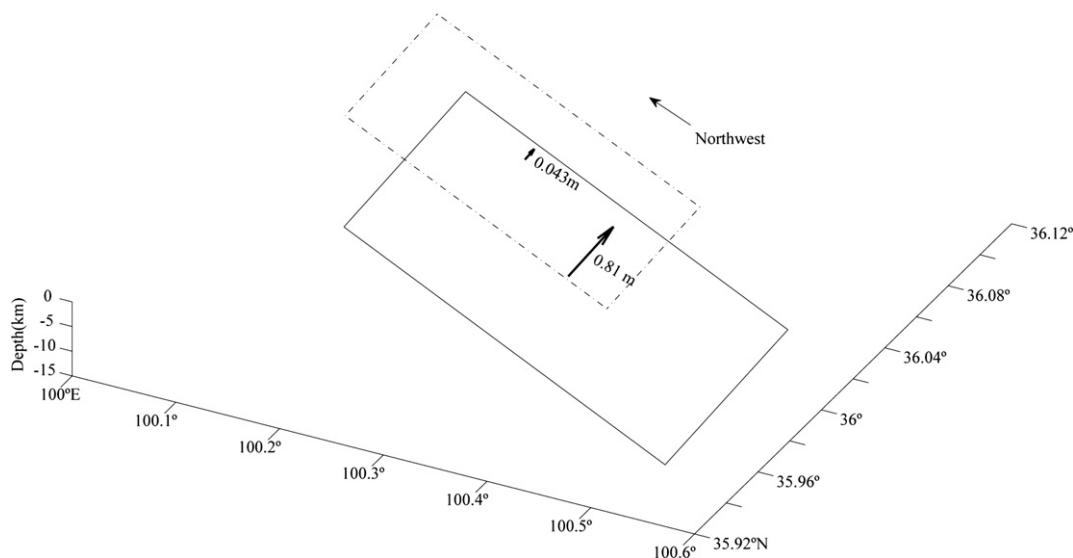


Fig. 6. Coseismic and afterslip fault planes. Rectangles with solid and chain lines are the coseismic and afterslip fault planes respectively. The arrows denote the inverted uniform coseismic slip and afterslip on fault.

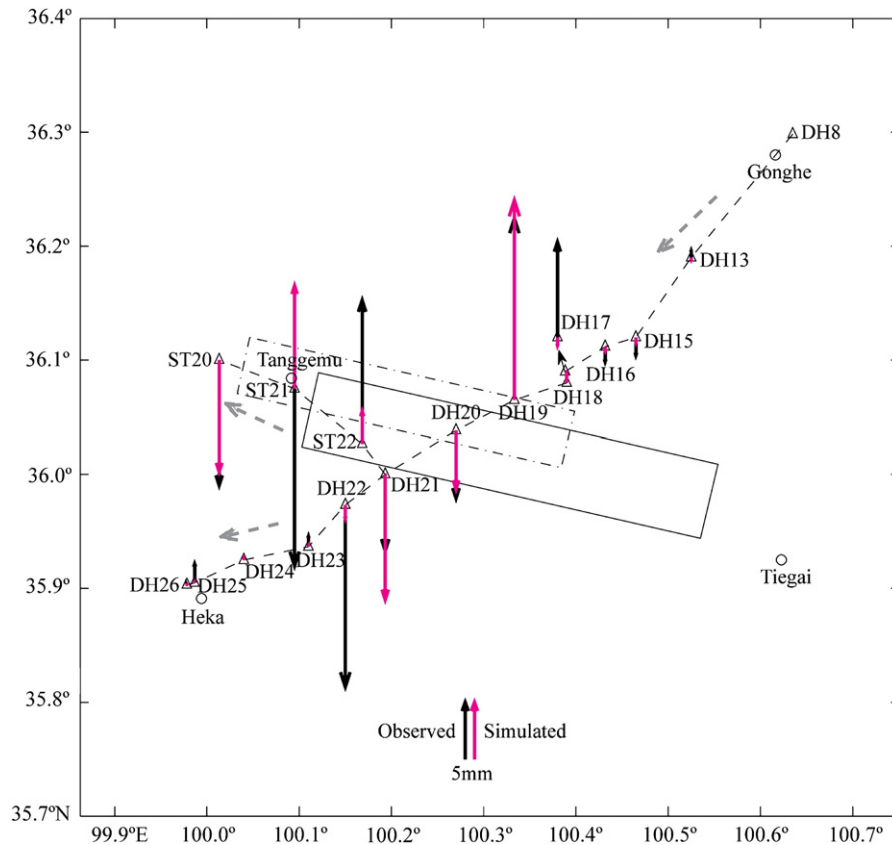


Fig. 7. Afterslip modeling result. Dashed gray arrows denote the directions of the leveling survey routes, elevation differences of two adjacent benchmarks are measured as the second benchmark elevation subtracting the first benchmark elevation along the leveling route. Vertical black arrows denote the adjusted logarithmic relaxation amplitudes, and pink arrows denote the model simulated results. Rectangles outlined with solid and dash-dotted lines are the surface projections of coseismic and postseismic fault plane models, respectively.

We simulate the absolute vertical displacements $h_i'(t)$ and $h_j'(t)$ at the locations of benchmarks i and j , respectively, at time t after the quake. The simulated elevation change between the two benchmarks is obtained as

$$h_{ij}'(t) = h_j'(t) - h_i'(t) \quad (5)$$

Subtracting Eq. (5) from Eq. (4) we have

$$\begin{aligned} res &= h_{ij} - h_{ij}' = [h_{ij}(t) - h_{ij}(t_0)] - [h_j'(t) - h_i'(t)] \\ &= h_{ij}(t) - [h_j'(t) - h_i'(t)] - h_{ij}(t_0) \end{aligned} \quad (6)$$

In Eq. (6), $h_{ij}(t_0)$ is unknown and the other three terms can be either measured or calculated. Adding up elevation difference of all the epochs between benchmarks i and j , we have

$$\sum_{m=1}^n res_m = \sum_{m=1}^n h_{ij}(t_m) - \sum_{m=1}^n [h_j'(t_m) - h_i'(t_m)] - nh_{ij}(t_0) \quad (7)$$

where n is the total epoch number of leveling surveys. If the modeling result is good, Eq. (7) will tend to approach zero. Therefore, it can be approximately considered

$$h_{ij}(t_0) = \left\{ \sum_{m=1}^n h_{ij}(t_m) - \sum_{m=1}^n [h_j'(t_m) - h_i'(t_m)] \right\} / n \quad (8)$$

We estimate $h_{ij}(t_0)$ using Eq. (8), and the result is adopted in Eq. (4) to deduce elevation differences for model constraints. The grid search is then used to find the best values of the unknown

parameters H and η (Fig. 9a). Our result yields the best estimates of the parameters $H = 20.5$ km (16.5–24 km at the 70% confidence level) and $\eta = 7 \times 10^{19}$ Pa·s (5×10^{19} – 1×10^{20} Pa·s at the 70% confidence level), respectively. The postfit residual χ^2 for viscoelastic relaxation is 9227.9 mm², and the reduced postfit residual χ^2 is 126.4 mm². Fig. 8 shows the comparisons between observed and model predicted elevation differences (asterisks).

5.3. Combined mechanism model

From the modeling results described above, we can see that the viscoelastic relaxation model fits data better than the afterslip model. However, the viscoelastic relaxation model still leaves a significant amount of data unexplained. Since the two models have quite different deformation origins, can the data be better explained if combining these two models together?

Following the method introduced in Sections 5.1 and 5.2, we employ a combined model incorporating both the afterslip and viscoelastic relaxation effects (but not the interactive effects between the two which are considered much less than themselves), and use the postseismic leveling data as constraints to search for the unknown parameters simultaneously. These parameters include the east and west extent and upper and lower depths of the fault patch undergoing afterslip, the amplitude of dip-slip component along the fault, the depth of the elastic upper crust, and the viscosity in the lower crust and upper mantle. We also conduct a grid search to find the best fit values of the unknown model parameters that minimize Eq. (1). Fig. 8 shows the comparisons between elevation differences and combined model results (triangles). Our result shows that the afterslip fault plane moved northwestward, with the left boundary moved 14.0 km (10.6–16.3 km at the 70% confidence level) and

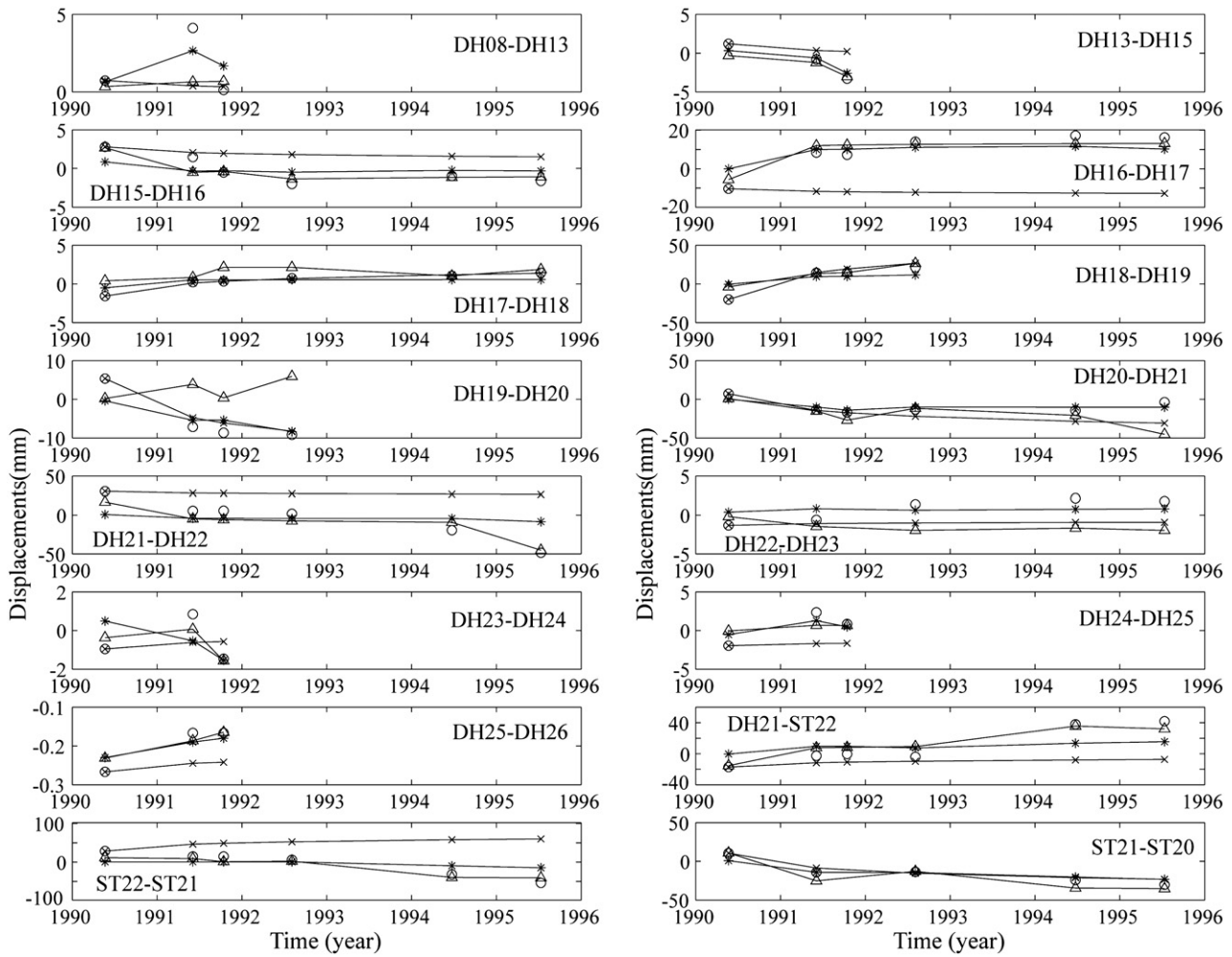


Fig. 8. Comparison between elevation differences and model predicted elevation differences. Circles denote the elevation differences, crosses are the prediction results of the afterslip model, asterisks denote the prediction results of the viscoelastic relaxation model, and triangles denote the prediction results of the combined model.

right boundary 22.1 (17.2–24.3 km at the 70% confidence level) km respectively. The upper and lower boundary extends 2.5 km (1.3–3.4 km at the 70% confidence level) and 3.5 (1.7–4.9 km at the 70% confidence level) km along the fault upward separately. The amplitude of reverse dip-slip along the fault is 0.031 ± 0.010 m. The depth of the upper crust is 21.5 km (17–23 km at the 70% confidence level) and the viscosity in the lower crust and upper mantle is 9×10^{19} Pa·s (7×10^{19} – 3×10^{20} Pa·s at the 70% confidence level). The data postfit residual χ^2 is reduced to 4929.7 mm² (Fig. 9B). This value is significantly less than the equivalent quantities of 23876.1 mm² for the afterslip model and 9227.9 mm² for the viscoelastic relaxation model, respectively. The reduced postfit residual χ^2 is now lowered to 72.5 mm². Therefore, using the combined afterslip and viscoelastic relaxation model we can satisfactorily explain the temporal and spatial vertical deformation observed postseismically at the earth's surface.

Table 3
Lithospheric structure model of Gonghe region.

Layer	Thickness (km)	Vp (km/s)	Vs (km/s)	Density (kg/m ³)	Viscosity (Pa·s)
1	0–H	5.70	3.30	2700	∞
2	H–∞	6.40	3.97	2890	η

6. Discussions

Using the observed postseismic vertical deformation data as constraints, we employ two mechanisms assuming deformation is caused by afterslip on fault and viscoelastic relaxation in media. The results indicate that the two mechanisms operate simultaneously to produce the postseismic vertical deformation at the surface. Afterslip occurred on the fault rupture plane of the main shock and its peripheral extensions, particularly upward to the sediment layer above the main rupture and westward along the original coseismic rupture. This may be because that the Gonghe basin has a relative thick sediment layer which behaves viscously, allowing the coseismic slip occurred on the fault plane underneath the sediment layer to propagate postseismically into the layer. This interpretation is similar to that of Lee et al. (2006), who studied postseismic deformation field of the 2003 Chengkung earthquake in Taiwan, and interpreted that postseismic creep was caused by strong velocity strengthening along the fault plane near the surface, which is associated with unconsolidated deposits in the footwall, mudstone the hanging wall, and sheared fault gouge in between. Lee et al. (2006) noted that thick sediments can play an important role in providing strong coupling (or velocity strengthening) on fault at shallow depth during the coseismic slip of a moderate sized earthquake (6.2–6.6). Coseismic rupture on fault of such an event tends to be weakened greatly at shallow depth because of the velocity strengthening effect, but coseismically

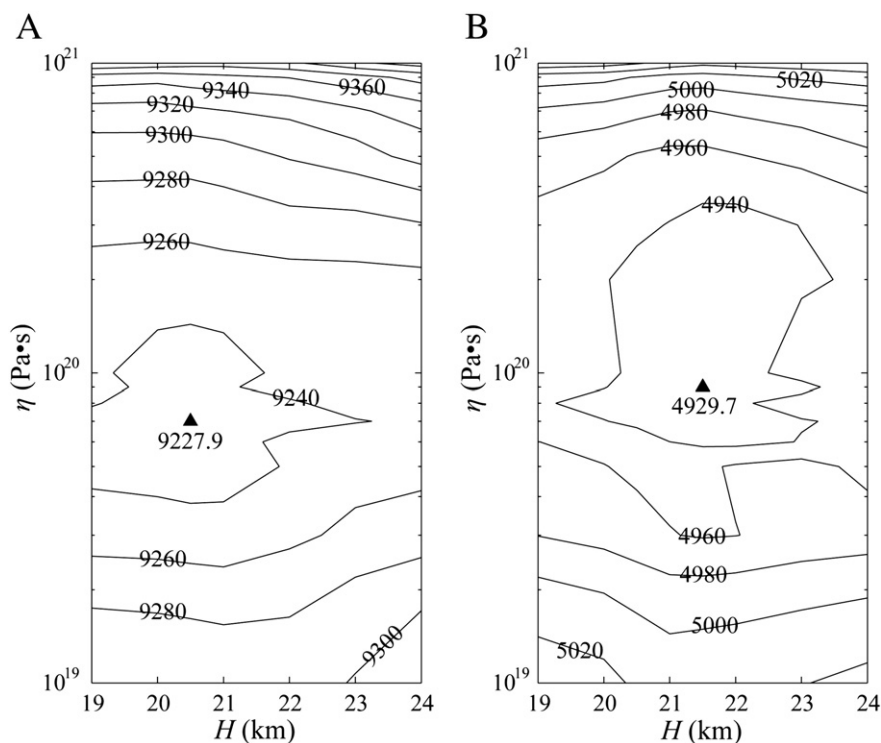


Fig. 9. Postfit residual χ^2 contour maps in H and η space. (A) Visco-elastic model; (B) combined mechanism model. The triangles indicate the best fit of the model.

increased Coulomb stress at this part of the fault will be released gradually after the quake, resulting in high postseismic creep. This has also been observed after the 1966 Parkfield earthquake (Scholz et al., 1969), the 1979 Imperial Valley earthquake (Cohn et al., 1982), the 1987 Superstition Hills earthquake (Williams and Magistrale, 1989), the 2003 Chengkung earthquake (Lee et al., 2006), and the 2004 Parkfield earthquake (Johanson et al., 2006). Postseismic deformation of the 1990 Gonghe earthquake attests again importance of rheological behavior of thick sediments on modulating slip process during and after a moderate sized earthquake.

The viscoelastic relaxation is considered to occur mainly in the lower crust and upper mantle. By grid search in the parameter space, we find that the depth of the elastic upper crust is ~ 21.5 km, which is consistent with the result given by Li and Chen (1996) and Xu and Chen (1997). The average viscosity of the lower crust and upper mantle is about 9×10^{19} Pa·s, which is nearly two orders of magnitude higher than the result estimated by Wang et al. (1996), who assumed the earth media as uniform half space. Differences between our result and the result of Wang et al. (1996) arise mainly from whether taking into account the contribution of afterslip and viscoelastic relaxation simultaneously. Our result demonstrates that a large part of slip after the earthquake took place in the sediment layer above the main rupture, which affected the near-field leveling observation in the epicentral region greatly. Because afterslip on this part of sediment decayed rather rapidly, ignoring afterslip effect and considering viscoelastic relaxation only to fit near-field observation data would result in grossly under-estimating the lower crust and upper mantle viscosity. The relatively high viscosity estimate for the lower crust and upper mantle underneath the Qaidam basin supports the notion that lithospheric structure at this part of the Tibetan Plateau is very much different from that in the Qiangtang region, south of the Kunlun Mountains. Lower crust and upper mantle region underneath the Qaidam basin is much more brittle and less viscous than the counterpart region of the Qiangtang domain, as revealed by the seismic tomography, shear-wave splitting, magnetotelluric, and postseismic deformation studies (Huang et al., 2003; McNamara et al., 1995; Wei et al., 2001; Tao et al., 2007). The faults

undergo reverse faulting in and around the Qaidam basin, therefore, may have deeper roots in mid crust, and strong coupling between the upper and lower crust may result in under thrusting in the lower crust and upper mantle, possibly beneath the Kunlun Mountains (Tapponnier et al., 2001). The deformation style in the Qaidam basin region is therefore in direct contrast with that south of the East Kunlun fault in the Qiangtang region (Shen et al., 2003).

7. Conclusions

In summary we have done the following in this study:

1. We updated the coseismic slip model of the 1990 Mw 6.4 Gonghe earthquake using leveling data, and find that the earthquake ruptured primarily through reverse faulting, with the dip and strike-slip components as 0.814 m and 0.014 m on the fault plane respectively.
2. We analyzed precise leveling observations measured repeatedly following the earthquake, and used a logarithmic or exponential relaxation function to characterize the temporal behavior of post-seismic deformation, obtaining the corresponding relaxation time constants as 0.165 year and 1.344 years, respectively.
3. We employed an approach utilizing the original form of the leveling data, i.e. the elevation differences between two adjacent benchmarks, not between a site and a reference point, as model constraints, reducing effectively biases introduced from cumulative errors propagated through data integration and making full use of the leveling data.
4. We developed a rheological deformation model to interpret the postseismic deformation of that earthquake. Our modeling result revealed significant afterslip on the coseismic rupture fault plane of the main shock and its peripheral extension, particularly upward into the sediment layer above the main rupture. It also inferred viscoelastic relaxation of the lower crust and upper mantle, with a viscosity of 9×10^{19} Pa·s. The result suggests more brittle and less viscous lower crust and upper mantle underneath the Qaidam basin than some of previous studies envisioned.

Acknowledgments

We are grateful to the survey team of the Second Monitoring Center, China Earthquake Administration for carrying out the postseismic leveling surveys under harsh working conditions. We also thank Jim Savage, an anonymous reviewer, and Hans Thybo, Editor-in-Chief of *Tectonophysics* for their constructive comments. This work was funded by the National Natural Science Foundation of China (No. 40974062, 41090294), the Ministry of Science and Technology of China (LED2009A02), the Seismic Research Foundation of CEA (200908029), and the National Science Foundation (EAR-0609656).

References

- Bürgmann, R., Ergintav, S., Segall, P., Hearn, E., McClusky, S., Reilinger, R., Woith, H., Zschau, J., 2002. Time-dependent distributed afterslip on and deep below the Izmit earthquake rupture. *Bulletin of the Seismological Society of America* 92, 126–137.
- Cohn, S.N., Allen, C.R., Gilman, R., 1982. Preearthquake and postearthquake creep on the Imperial fault and the Brawley fault zone. The Imperial Valley, California, Earthquake of October 15, 1979, 161–167.
- Chen, Y.T., Xu, L.S., Li, X., Zhao, M., 1996. Source process of the 1990 Gonghe, China, earthquake and tectonic stress field in the Northeastern Qinghai–Xizang (Tibetan) Plateau. *Pure and Applied Geophysics* 146, 697–715.
- Huang, Z.X., Su, W., Peng, Y.J., Zheng, Y.J., Li, H.Y., 2003. Rayleigh wave tomography of China and adjacent regions. *Journal of Geophysical Research* 108. doi:10.1029/2001JB001696.
- Johanson, I.A., Fielding, E.J., Rolandone, F., Bürgmann, R., 2006. Coseismic and postseismic slip of the 2004 Parkfield earthquake from space-geodetic data. *Bulletin of the Seismological Society of America* 96, 269–282.
- Lee, J.-C., Chu, H.-T., Angelier, J., Hu, J.-C., Chen, H.-Y., Yu, S.-B., 2006. Quantitative analysis of surface coseismic faulting and postseismic creep accompanying the 2003, $M_w = 6.5$, Chengkung earthquake in eastern Taiwan. *Journal of Geophysical Research* 111, B02405. doi:10.1029/2005JB003612.
- Li, X., Chen, Y.T., 1996. Inversion of long-period body-wave data for the source process of the Gonghe, Qinghai, China earthquake. *Acta Seismologica Sinica* 18, 279–286 (in Chinese).
- Marone, C., Scholz, C.H., Bilham, R., 1991. On the mechanics of earthquake afterslip. *Journal of Geophysical Research* 96, 8441–8452.
- McNamara, D.E., Owens, T.J., Walter, W.R., 1995. Observations of regional phase propagation across the Tibetan Plateau. *Journal of Geophysical Research* 100, 22215–22229.
- Nur, A., Mavko, G., 1974. Postseismic viscoelastic rebound. *Science* 183, 204–206.
- Okada, Y., 1992. Internal deformation due to shear and tensile faults in a half-space. *Bulletin of the Seismological Society of America* 82, 1018–1040.
- Owen, S., Anderson, G., Agnew, D.C., Johnson, H., Hurst, K., Reilinger, R., Shen, Z.K., Svarc, J., Baker, T., 2002. Early postseismic deformation from the 16 October 1999 Mw 7.1 Hector Mine, California, earthquake as measured by survey-mode GPS. *Bulletin of the Seismological Society of America* 92, 1423–1432.
- Person, W.J., 1991. Seismological notes – March–April 1990. *Bulletin of the Seismological Society of America* 81, 297–302.
- Pollitz, F.F., 1997. Gravitational viscoelastic postseismic relaxation on a layered spherical earth. *Journal of Geophysical Research* 102, 17921–17941.
- Reilinger, R., 1986. Evidence for postseismic viscoelastic relaxation following the 1959 M = 7.5 Hebgen Lake Montana Earthquake. *Journal of Geophysical Research* 91, 9488–9494.
- Scholz, C.H., Wyss, M., Smith, S.W., 1969. Seismic and aseismic slip on the San Andreas fault. *Journal of Geophysical Research* 74, 2049–2069.
- Shen, Z.K., Jackson, D., Feng, Y., Cline, M., Kim, M., Feng, P., Bock, Y., 1994. Postseismic deformation following the Landers earthquake, California, 28 June, 1992. *Bulletin of the Seismological Society of America* 84, 780–791.
- Shen, Z.K., Wang, M., Gan, W., Zhang, Z., 2003. Contemporary tectonic strain rate field of Chinese continent and its geodynamic implications. *Earth Science Frontiers* 10, 93–100 (in Chinese).
- Shi, X.J., Wen, D., Bao, X.Y., Li, C.B., Huang, Y., 2006. Application of rock creep experiment in calculating the viscoelastic parameters of earth medium. *Science in China, Series D: Earth Sciences* 49, 492–498.
- Tao, W., Shen, Z.K., Wan, Y.G., Shan, X.J., Ma, C., 2007. Crustal elasticity contrast across the East Kunlun fault in northern Tibet inferred from InSAR measurements of the 2001 Mw 7.8 Kokoxili earthquake. *Chinese Journal of Geophysics* 50, 658–665.
- Tapponnier, P., Xu, Z., Roger, F., Meyer, B., Arnaud, N., Wittlinger, G., Yang, J., 2001. Obligate stepwise rise and growth of the Tibet Plateau. *Science* 294, 1671–1677.
- Tu, D.L., 1992. The study on the structural environment and seismogenesis of the Gonghe earthquake 6.9 on April, 26, 1990. *Plateau Earthquake Research* 4, 15–22 (in Chinese).
- Ueda, H., Ohtake, M., Sato, H., 2001. Afterslip on the plate interface following the 1978 Miyagi-Oki, Japan, earthquake, as revealed from geodetic measurement data. *Tectonophysics* 338, 45–57.
- Wang, W.P., Wang, Q.L., 1998. Dislocation parameters of Gonghe earthquake jointly inferred by using genetic algorithms and least squares method. *Acta Seismologica Sinica* 21, 285–290 (in Chinese).
- Wang, Q.L., Gong, S.W., Zhang, X., Zhu, Y.Q., 1996. Effective relaxation time and viscosity of the earth inferred from the postseismic vertical deformations of the 1990 Ms 7.0 Gonghe earthquake. *Acta Seismologica Sinica* 19, 480–486 (in Chinese).
- Wang, R., Lorenzo-Martin, F., Roth, F., 2006. PSGRN/PSCMP—a new code for calculating co- and post-seismic deformation, geoid and gravity changes based on the viscoelastic-gravitational dislocation theory. *Computers & Geosciences* 32, 527–541.
- Wei, W., Unsworth, M., Jones, A., et al., 2001. Detection of widespread fluids in the Tibetan crust by magnetotelluric studies. *Science* 292, 716–718.
- Williams, P.L., Magistrale, H.W., 1989. Slip along the Superstition Hills fault associated with the 24 November 1987 Superstition Hills, California, earthquake. *Bulletin of the Seismological Society of America* 79, 390–410.
- Xu, L.S., Chen, Y.T., 1997. Source parameters of the Gonghe, Qinghai Province, China, earthquake from inversion of digital broadband waveform data. *Acta Seismologica Sinica* 19, 113–128.
- Zhao, M., Chen, Y.T., Gong, S.W., Wang, Q.L., 1992. Inversion of focal mechanism of Gonghe earthquake in April 26, 1990 using leveling data. *Crustal Deformation and Earthquake* 12, 1–11 (in Chinese).